INTEGRATION OF HYDROGEL MICROFIBERS FOR HYBRID LEAD SEQUESTRATION AND SENSING IN CROP PLANTS: A NOVEL APPROACH FOR PHYTOREMEDIATION

*Rhythem Tahrin, Francisco Perez, Mohammad Solaiman, Md Najmul Islam, Shah Zayed Riam, and Shawana Tabassum**

The University of Texas at Tyler, Tyler, TX, USA

ABSTRACT

This paper reports biodegradable microfibers (μF) synthesized from sodium alginate and carboxymethyl cellulose and inserted into a plant's stem for simultaneous capture and monitoring of lead. The high surface area of the μF enhances lead capture efficiency by increasing adsorption sites. In vitro experiments using a 3D printed tube simulating the plant's vascular system demonstrated the μF's ability to sequester lead ions and exhibit corresponding impedance changes. Microscopy and spectroscopy results confirmed ~12% lead adsorption by the μF. During in situ testing, impedance measurements conducted with μF implanted into the plant's vascular bundle confirmed lead adsorption, reflecting the findings observed in vitro. Future research will investigate effects on plant physiology and adaptation of the μF for capturing other contaminants.

KEYWORDS

Biodegradable microfibers, lead sequestration, impedance sensing, in-situ monitoring, phytoremediation, crop plants.

INTRODUCTION

Lead (Pb) contamination is a significant environmental concern due to its widespread presence and harmful effects on human health and ecosystems. It is the second most toxic metal, persistent, and highly hazardous. Both natural processes and human activities, such as industrial operations (e.g., mining, smelting, and other manufacturing processes) and the use of Pb-containing products (e.g., batteries, paints, and gasoline additives), contribute to Pb pollution. Anthropogenic sources, including industrial processes and product usage, are the primary contributors to environmental contamination [1]. These activities release Pb into soil, water bodies, and the atmosphere, entering the food chain through various pathways. Once absorbed by plants in agricultural systems, Pb accumulates in the leaves, stems, fruits, and vegetables [2]. According to the World Health Organization (WHO), the provisional tolerable weekly intake (PTWI) for Pb is 0.025 ppm, with a maximum allowable concentration of 0.1 ppm in fruiting vegetables, excluding Cucurbits [3]. Alarmingly, some tomato plants have been found to have an average Pb concentration of 5.5 ppm, exceeding the permissible limit by 55 times [4].

Roots are the primary site of metal uptake in plants [5]. Pb present in soil water is assimilated by the roots, traverses multiple cell membranes, reaches the xylem, and spreads along the water movement path driven by the transpiration pull. Pb uptake in plants is influenced by the physiological and chemical conditions of soil, plant species, and genotypes. In a study conducted on the greenhouse soil, Murtić et al. concluded that alkaline soil and a higher Pb concentration in the soil increase plant's contamination [6]. Pb toxicity in plants exhibits various detrimental effects, including inhibited root growth, stunted development, and chlorosis. It interferes with chlorophyll synthesis, hampers photosynthesis, disrupts mineral nutrition and water balance, and at high levels, induces cell death and oxidative stress, affecting normal physiological functions. These disruptions can lead to reduced seed germination, hindered growth, and impaired nutrient absorption. The severity of these effects depends on Pb concentration and exposure duration [7]. Contamination of edible parts poses a direct risk to humans and animals, potentially causing severe health issues, especially in children, such as developmental delays, neurological disorders, cognitive impairments, and behavioral problems [8].

Phytoremediation, the use of plants to remove contaminants from soil or water, has been explored as a solution for Pb remediation [9]. However, the traditional phytoextraction methods, which rely on plants absorbing and accumulating contaminants in their tissues, lead to the translocation of absorbed Pb from the roots to the edible parts. Furthermore, only specific plants are capable of phytoremediation [10]. However, adsorption shows promise for efficiently and cost-effectively treating wastewater with low Pb concentrations [11]. Sodium alginate (SA) is a natural polysaccharide primarily composed of mannuronic acid (M) and guluronic acid (G), featuring numerous free carboxyl groups (−COO−). It acts as a polymeric flocculant with a high adsorption capacity and can form a stable gel by reacting with various divalent and trivalent cations such as Ca^{2+}, Ba^{2+}, and Fe^{3+} [12].

Existing literature reports hydrogel structures in spherical or sheet forms, which can capture heavy metals. Tang et al. studied the adsorption of cadmium (Cd(II)) and copper (Cu(II)) using novel thermosensitive hydrogel microspheres composed of aminated sodium alginate and poly-N-isopropyl acrylamide (NH_2-SA/PNIPA) [13]. The study demonstrated that NH_2-SA/PNIPA exhibited higher adsorption efficiency under conditions of interfering monovalent cations and neutral pH, with adsorption capacities of 57.2 mg g^{-1} for Cu(II) and 100.5 mg g^{-1} for Cd(II). The adsorption process was mainly controlled by the complexation reaction, and the hydrogel microspheres showed high diffusibility and reusability. Wang et al. reported a water droplet templating polymerization strategy to synthesize dithiocarbamate-decorated poly(vinyl amine) hydrogel beads (DTC-Fe_3O_4@PVAM) for heavy metal ion removal [14]. The stable C–N cross-linked polymeric network provided resilience to harsh chemical conditions and exhibited excellent fatigue resistance in the hydrogel beads. Incorporating chelating DTC groups and Fe_3O_4 nanofillers enhanced adsorption capacities, foreign ion resistance, magnetic separation, and reusability of the adsorbent material. Ren et al. prepared sodium alginate–carboxymethyl cellulose (SA–CMC) gel beads for efficient Pb(II) removal [15]. Static adsorption experiments demonstrated that Pb(II) adsorption by SA–CMC exceeded 99% under highly optimized conditions, and the removal efficiency was significantly higher than that of conventional adsorbents. Song et al. developed a bioinspired strategy to fabricate super-adsorbent hydrogel spheres (SAHSs) using self-sacrificing micro-reactors [16]. The poly(2-acrylamido-2-methyl-propanesulfonic acid-co-acrylic acid) hydrogel spheres exhibited outstanding adsorption capabilities for heavy metal ions (4312 ± 185 mg g^{-1} for Pb(II)). An adsorption column packed with SAHSs effectively purified 6280 mL of dye-containing wastewater (150 μmol L^{-1}) using only 7 mL of SAHSs. The hydrogel spheres also showed good recyclability, dynamic filtration–regeneration, selective adsorption, and smart separation–regeneration properties.

The studies by Tang et al., Song et al., Wang et al., and Ren et

978-1-940470-05-4/HH2024/$25©2024TRF
DOI 10.31438/TRF.HH2024.36

al. have made notable contributions to the development of hydrogel-based adsorbents for heavy metal ion removal. However, these studies have some limitations that must be addressed for practical applications. Tang et al. and Wang et al. utilized complex synthesis procedures that may pose challenges for large-scale production. Song et al.'s bioinspired strategy involves specialized fabrication processes, potentially requiring cost-effectiveness improvements for widespread implementation. Ren et al. prepared hydrogel beads through a multi-step process of blending and cross-linking, which is time-consuming and labor-intensive. Moreover, the specific morphologies of these hydrogel-based adsorbents and the need for efficient separation and regeneration processes may limit their application in field conditions. Addressing these limitations is essential for enhancing the practical use of hydrogel-based adsorbents for heavy metal ion removal.

In contrast, we report μF that are synthesized by tuning the viscosity of the SA-CMC dispersion and extruding it continuously into a crosslinking solution. The μFs are engineered to a size suitable for insertion into the plant's vascular bundle. The high surface area to volume ratio of these μF enhances the lead capture efficiency by offering abundant active sites for adsorption. Unlike traditional phytoremediation methods relying on phytoextraction, our approach intervenes directly in the plant's internal xylem vessels to sequester lead near the roots, preventing aerial contamination. Additionally, we employ a hybrid approach, continuously monitoring lead adsorption by the μF and enabling timely alerts for intervention.

MATERIALS AND METHODS

2.1 Materials and reagents

Sodium Alginate (SA), Carboxymethyl cellulose (CMC), Calcium Chloride ($CaCl_2$), Ferric Chloride ($FeCl_3$), Copper (II) sulfate pentahydrate ($CuSO_4$. $5H_2O$) and Lead Nitrate ($PbNO_3$) all are purchased from Sigma Aldrich, USA and are research grade.

2.2 Viscosity tuning and syringe pump calibration

A MATLAB script was developed to compute the required dynamic viscosity of the SA-CMC hydrogel and the optimal fluid velocity at the needle tip to produce fibers with a target diameter of 50 μm. The script models the free vortex flow generated by a magnetic stirrer using the following equation [17]:

$$v_{needleTip} = k \div r_{from\_center} \quad (1)$$

where $v_{needleTip}$ is the fluid velocity at the needle tip, k is a constant of proportionality, and r_{from_center} is the radius from the center of the stirrer to the needle tip. k is determined using the angular velocity (ω) of the stirrer set at 1100 rpm, converted to radians per second ($\omega = 2\pi \times$ rpm / 60) and r_{from_center} (=25 mm). k is calculated as:

$$k = \omega (r_{from\_center})^2 \quad (2)$$

The script assumes that a spherical bead forms at the tip of the needle and is then extruded by the fluid velocity. It also assumes that the drag force acting on the bead upon detachment from the needle tip equals the viscous force. The drag force (F_{drag}) is calculated using the drag coefficient for a sphere in laminar flow regime (C_d = 24), the density of water (ρ = 1000 kg/m³), the fluid velocity at the needle tip ($v_{needleTip}$), and the radius of the bead (r_{bead}):

$$F_{drag} = 0.5\rho (v_{needleTip})^2 C_d \pi (r_{bead})^2 \quad (3)$$

The viscous force ($F_{viscous}$) acting on the bead is described by Stokes' law, which relates the frictional force exerted on a small sphere moving through a viscous fluid to the dynamic viscosity of the fluid:

$$F_{viscous} = 6\pi\mu (v_{needleTip}) (r_{bead}) \quad (4)$$

where μ is the dynamic viscosity of the fluid and r_{bead} is the radius of the bead. By equating the drag force (Equation 3) to the viscous force (Equation 4), the script solves for the required dynamic viscosity (μ) of the SA-CMC hydrogel:

$$\mu = \rho v_{needleTip} C_d r_{bead} / 12 \quad (5)$$

The MATLAB script outputs the required dynamic viscosity of the SA-CMC hydrogel (μ) to form beads that extrude into fibers with a diameter of 50 μm. These findings provide an initial estimate of the hydrogel viscosity for the desired fiber diameter, guiding further optimization. The script simplifies by assuming a perfectly spherical bead formation, equal drag and viscous forces at bead detachment, and using a drag coefficient for a sphere in laminar flow. It also assumes a constant fluid velocity at the needle tip, which may not fully capture the fluid dynamics complexities. Factors like surface tension, hydrogel viscoelasticity, and needle diameter influence final fiber properties and should be considered during optimization.

2.3 Microfiber synthesis

After achieving the target viscosity of 0.028798 Pa.s using the developed MATLAB script, various SA and CMC ratio solutions were prepared and their viscosity measured with an NDJ-9S Viscosity Meter Rotational Viscometer. The desired weight ratio of SA to CMC was determined through trial and error. To synthesize μFs, 5000 mg of SA and CMC each were dissolved in 400 ml of distilled water and stirred overnight until homogeneous [15]. A specialized setup with a syringe pump from New Era Pump Systems Inc., USA was used for synthesizing μFs at a flow rate of 0.10 ml/min, determined through iterative experimentation. The syringe needle, attached to an extended tube, was submerged into a magnetically stirred solution of 1000 mg $CaCl_2$ in 100 ml distilled water. This $CaCl_2$ solution served as a crosslinking agent for the SA: CMC solution, aiding in the formation of a fibrous structure as it exited the nozzle. Following the initial crosslinking, the fibers were further crosslinked in a solution of 1000 mg $FeCl_3$ and 100 ml distilled water, stirred for 24 hours. Subsequently, the fibers were washed with distilled water to remove excess crosslinking solution, and any remaining solution was sucked by a syringe.

RESULTS AND DISCUSSION

3.1 Microscopic and spectroscopic characterizations

Optical microscopic images with Leica TL5000 Ergo Transmitted light base demonstrated the fibrous structure of the *μF* (Figure 1). This methodology ensures reproducibility and integrity of the synthesized μF for further analysis and application.

Scanning Electron Microscopy (SEM) was used to examine the internal structure of the synthesized μF, revealing a spiral shape with an average diameter of 35μm as shown in Figure 2a. The high surface area of the dense network of intertwined fibers enhances Pb

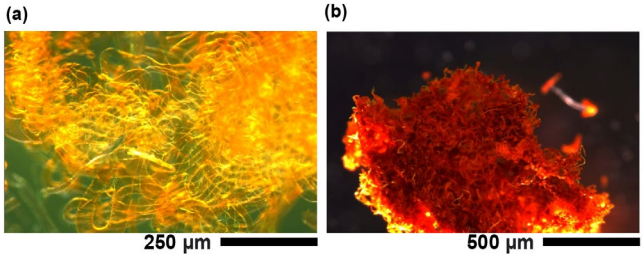

Figure 1. Optical microscopic images of the synthesized μF with a magnification of (a)250 μm and (b)500 μm.

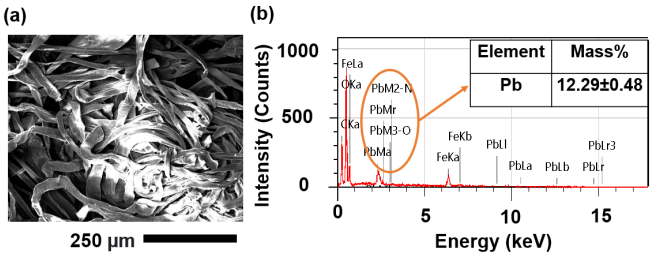

Figure 2. (a) SEM and (b) EDS results of the synthesized microfibers. The inset in (b) shows the % of Pb^{2+} adsorption by µF.

capture efficiency. Although µF were targeted to have a diameter of 50 µm, they were observed to have an average diameter of 35 µm. This deviation may be attributed to fluctuations in experimental conditions, such as temperature and humidity, variations in solution properties like viscosity and surface tension, as well as differences in equipment calibration. Additionally, the molecular weight and chain conformation of the polymer could have resulted in this deviation. Moreover, Energy Dispersive Spectroscopy (EDS) was performed to assess the adsorption of Pb^{2+} ions (Figure 2b).

3.2 Effects of vibration on Pb adsorption

The synthesized µF were subjected to vibration to evaluate their Pb adsorption capacity. First, a 1000 ppm of $PbNO_3$ solution was prepared. Next, the synthesized µF were immersed in the $PbNO_3$ solution in two separate beakers: one subjected to stirring at 250 rpm for 18 hours and the other kept stationary. The adsorption of Pb by the µF was measured in both scenarios to assess the effects of vibration on Pb adsorption. The EDS analysis revealed that the µF subjected to vibrations exhibited a Pb^{2+} adsorption percentage of 18%, whereas those without vibrations displayed a slightly lower adsorption percentage of approximately 12%, as depicted in Figure 2b. These results infer that even without vibration, the µF can adsorb Pb^{2+} ions, suggesting their inherent adsorption capability.

3.3 In vitro experimental setup

An in-vitro setup was designed to evaluate Pb adsorption and resulting impedance variations of the µF (Figure 3). A 30 mm long tube with internal sieves, replicating the plant's vascular bundle, was printed using the Form 3+ 3D printer from Formlabs, USA. A custom setup with a syringe pump was used to apply a reverse pumping flow to the 3D printed tube at a 200 µl/min rate, imitating water flow inside a tomato plant's vascular system [18]. The µF were positioned within the sieves of the 3D printed tube, and the syringe pump allowed the flow of three solutions: distilled water, $PbNO_3$ solution, and a salt solution containing $CuNO_3$, $PbNO_3$, and $CaCl_2$.

Two conductive probes, shown in Figure 3, were inserted into the sieve part to enable continuous impedance measurements of µF. These measurements were recorded using an Applent Instruments AT3B17A Precision LCR meter while solutions flowed through the µF within the 3D printed tube. The conductive probes made contact with the µF inserted inside the sieve. Following impedance measurements, the µF were extracted from the tube for further characterization. The EDS results revealed that the µF exhibited a Pb adsorption capacity of approximately 9%, as illustrated in Figure 4a-b. This seemingly low percentage can be attributed to the relatively small amount of Pb^{2+} compared to other elements present in the test solution. Additionally, the EDS analysis was limited to a very small region on a 50 µm scale, potentially restricting the measurement of the µF's complete adsorption potential.

Impedance measurements were continuously recorded during the testing with different solutions (Figure 4c). The initial impedance measurement of the µF served as a reference point.

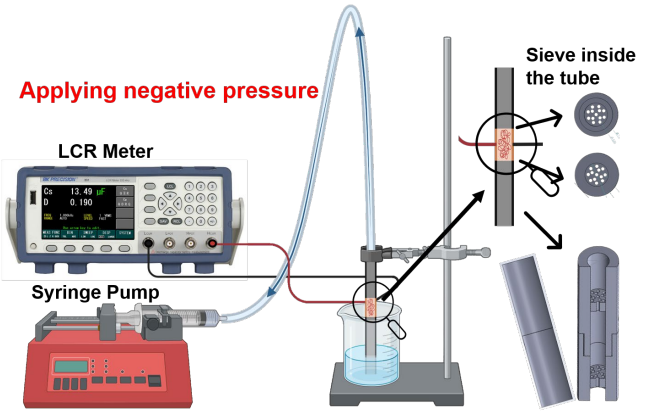

Figure 3. In-vitro experimental setup. A syringe pump is used to apply negative pressure to the 3D printed tube to pull the water upwards. An LCR meter was used to measure the impedance of µF.

As distilled water flowed through the µF, impedance exceeded 10^5 Ω, indicating low conductivity of the µF. In contrast, when $PbNO_3$ solution passed through the µF, the impedance decreased, implying the capture of Pb^{2+} ions by the µF. Finally, the passage of the salt mixture ($CuNO_3$, $PbNO_3$, and $CaCl_2$) through the µF resulted in the most significant impedance drop, as the solution contained the highest concentration of ions from various elements. These impedance measurements demonstrate the potential of the µF to function as a biosensor, with their impedance changing in response to Pb adsorption. This capability could be further developed to create a sophisticated biosensing system capable of real-time monitoring and detection of Pb^{2+} ions in various environments.

3.4 In situ testing in live plants

For the in-situ testing, Pb adsorption efficacy of the synthesized µF was evaluated in live tomato plants. A small incision, approximately 1-1.5 mm in length, was made in a non-critical area about 2-3 cm above the soil surface using a syringe as demonstrated in Figure 5a, and the µF were gently inserted into the incised area. Subsequently, a 1000 ppm $PbNO_3$ solution was applied to the soil

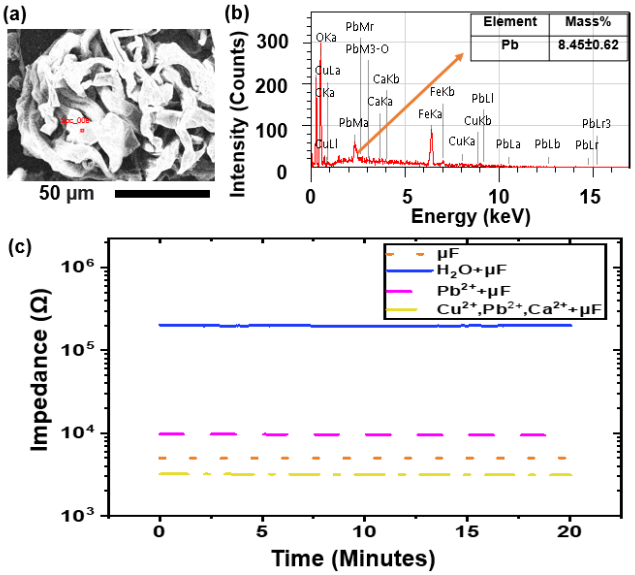

Figure 4. (a) SEM and (b) EDS results of the µF following the in-vitro test. The inset in (b) shows the % of Pb^{2+} adsorption by µF. (c) Continuous measurements of impedance of the µF during ion uptake by the tube.

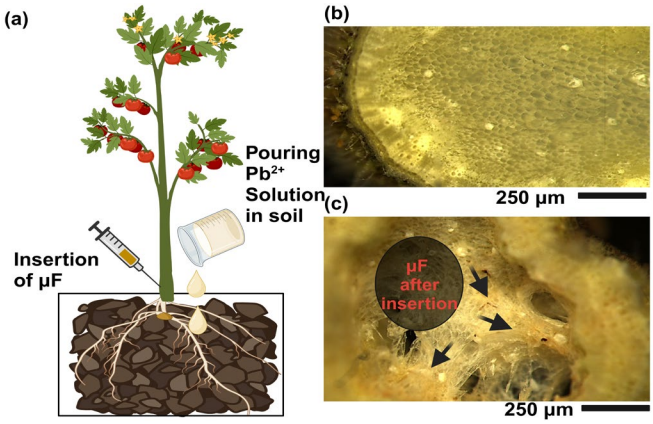

Figure 5. (a) Schematic illustration of µF injection inside the stem and Pb^{2+} uptake by the roots. Microscopic images of the cross section of a tomato stem (b) before and (c) after the µF injection into the vascular bundle.

surrounding the plant. After an incubation period of 18 hours, the µF were carefully extracted from the plant for microscopic and EDS analysis. Figure 5b displays the cross-section of a tomato plant stem under the microscope without inserted µF, providing a baseline for comparison with Figure 5c, which shows the anticipated presence of µF post-insertion. These microscopic images elucidate the presence and distribution of the injected µF within the vascular bundle. Furthermore, the EDS results in Figure 6a-b showed that the µF extracted from the incised plant exhibited Pb adsorption capacity of approximately 11%, validating their efficacy in real plant environments. The EDS analysis also detected traces of other elements such as Mo and Ca in the µF, indicating the complex nature of ion adsorption processes in live plants.

Impedance measurements were also conducted to assess the uptake of Pb ions by the plant and their adsorption by the µF. The impedance of the plant was initially measured with an LCR meter to establish a baseline, yielding a value of 10^4 Ω. Subsequently, after the injection of µF, the impedance decreased, indicating the

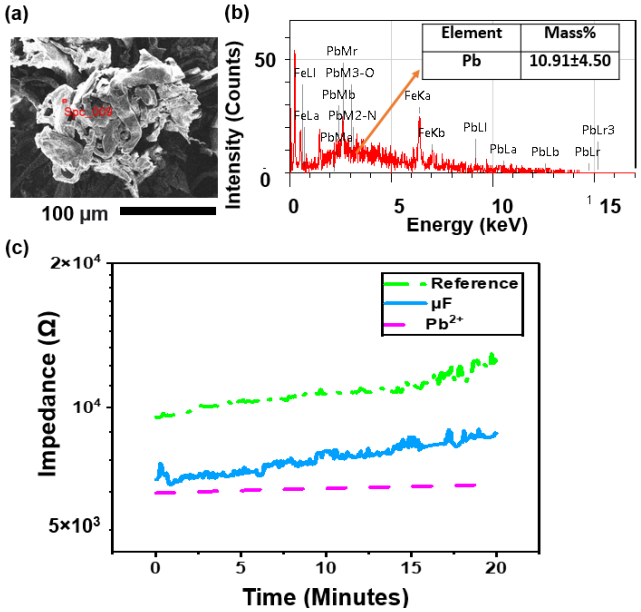

Figure 6. (a) SEM and (b) EDS results of the µF following the in-situ test in a tomato plant. The inset in (b) shows the % of Pb^{2+} adsorption by µF. (c) Continuous measurements of impedance of the µF during ion uptake by the plant.

presence of the µF. Following an 18-hour wait period, during which it was anticipated that the plant would adsorb Pb, the impedance further decreased. This reduction in impedance serves as evidence of Pb adsorbed by the µF, as illustrated in Figure 6c.

Furthermore, we investigated whether the µF remained in their original site of insertion or moved downstream as the plant grew over time. Microscopic images were taken after 12 days of insertion of the µF into the vascular bundle. It was observed that the µF remained in their original insertion site without significant movement, as shown in Figure 7a-b. No µF were observed 2mm above (Figure 7c) or 2mm below (Figure 7d) the site of insertion.

Another experiment was conducted to identify the correlation between the impedance measurements and the amount of lead uptaken by the plants. Different concentrations of Pb^{2+} (1000 ppm, 800 ppm, 600 ppm, and 400 ppm) were added to the soil of four tomato plants, with each solution allowed to sit for 24 hours. These concentrations were selected based on literature indicating that the average Pb concentration in tomato plants is about 5.5 ppm [4], which is roughly 5% of the Pb content in the soil [1]. Impedance values were measured before (denoted as R) and after 24 hours of Pb exposure (denoted as Pb). Notably, a reduction in impedance occurred following Pb exposure, indicating successful Pb^{2+} adsorption by the µF at each Pb concentration. These results are shown in Figure 8a. The impedance variations versus Pb concentration plot in Figure 8b further shows their correlation.

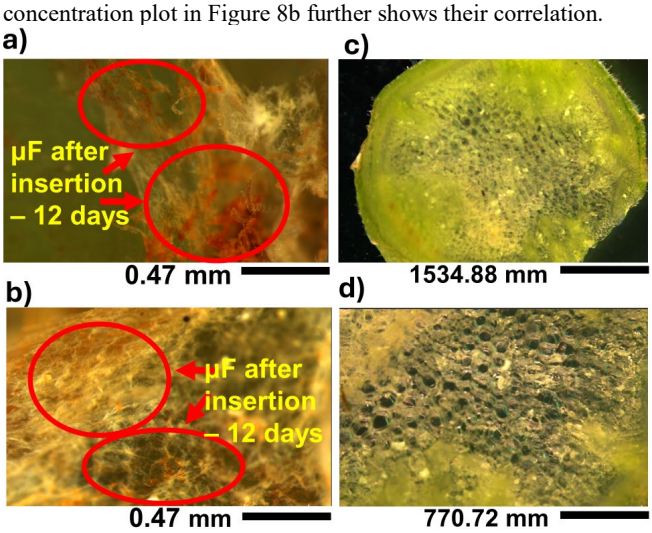

Figure 7. Microscopic images of the cross section of a tomato stem at (a)-(b), 2mm above (c), and 2mm below (d) the µF insertion site.

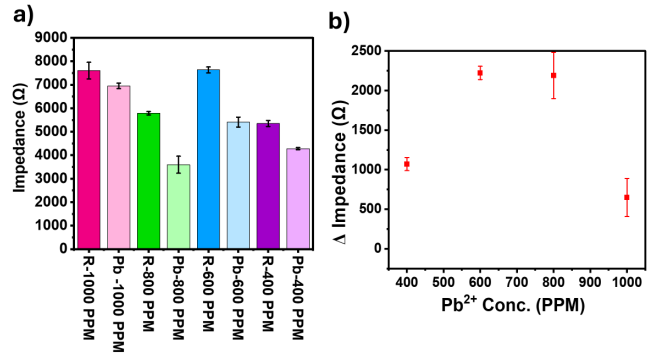

Figure 8. (a) Impedance measurements for varying concentrations of Pb^{2+} solutions. Here, R = Reference impedance of the µF inserted inside the plant before Pb exposure and Pb = Impedance of the µF after 24 hours of Pb exposure. (b) Impedance variation vs. Pb^{2+} concentrations. Error bars represent 3 independent measurements.

CONCLUSION AND FUTURE DIRECTIONS

In conclusion, the synthesized μF exhibited promising capabilities for environmental remediation and plant nutrition applications. Through a series of tests, including in vitro and in situ experiments, the μF demonstrated a high adsorption capacity for Pb^{2+} ions. These results indicate that the μF can effectively adsorb Pb^{2+} ions in both simulated and live plants. In vitro tests showed that the μF could adsorb Pb^{2+} ions even in the absence of vibration, suggesting inherent adsorption capabilities of the μF. In the in-situ tests involving μF insertion into tomato plants, significant Pb^{2+} ion adsorption occurred after soil exposure to $PbNO_3$ solution, which was further confirmed by the continuous impedance measurements. Additionally, the presence of other elements such as Molybdenum (Mo) and Calcium (Ca) in the μF, as detected by EDS, indicates the complex nature of ion adsorption processes in natural settings. Overall, these findings suggest that the synthesized μF have the potential to be developed into a biosensor system for monitoring and detecting Pb ions in environmental and agricultural settings. Further research is needed to optimize the synthesis process and explore additional applications of these μF.

Future research will focus on enhancing the application and effectiveness of synthesized μF. One research avenue is the optimization of the synthesis process to improve the adsorption capacity and selectivity of the μF to Pb^{2+} ions. This could involve fine-tuning the composition and structure of the μF to enhance their performance in real-world environments. Additionally, further research could focus on the development of a fully integrated biosensor system based on the μF. This could involve incorporating the μF into a needle-structured sensor platform that would be entirely wearable to the plant [19]-[21]. Exploring the potential use of μF in combination with other materials or technologies could also be beneficial. For example, μF could be combined with nanomaterials to enhance their adsorption capacity or integrated into smart irrigation systems for precise and efficient nutrient delivery to plants. Overall, these future directions have the potential to significantly advance the field of sustainable and climate-smart agriculture, providing innovative solutions for addressing heavy metal contamination and enhancing crop productivity.

ACKNOWLEDGEMENTS

This work is supported in part by the National Science Foundation under Grant No: 2138701 and in part by the VentureWell Grant 21716-20.

REFERENCES

[1] A. Kumar et al., "Lead toxicity: health hazards, influence on food chain, and sustainable remediation approaches.," Int. J. Environ. Res. Public Health, vol. 17, no. 7, Mar. 2020.

[2] A. Kumar and M. N. V. Prasad, "Plant-lead interactions: Transport, toxicity, tolerance, and detoxification mechanisms.," Ecotoxicol. Environ. Saf., vol. 166, pp. 401–418, Dec. 2018, doi: 10.1016/j.ecoenv.2018.09.113.

[3] "Codex General Standard for Contaminants and Toxins in Food and Feed," Codex Stan 193-1995, adopted 1995; revised 1997, 2006, 2008, 2009; amended 2009, 2010.

[4] C. V. Mohod, "A Review on the Concentration of the Heavy Metals in Vegetable Samples like Spinach and Tomato Grown Near the Area of Amba Nalla of Amravati City," Int. J. Innov. Res. Sci. Eng. Technol., vol. 4, no. 5, pp. 2788, May 2015.

[5] E. P. Colangelo and M. L. Guerinot, "Put the metal to the petal: metal uptake and transport throughout plants.," Curr. Opin. Plant Biol., vol. 9, no. 3, pp. 322–330, Jun. 2006.

[6] S. Murtic, C. Zahirovic, H. Civic, L. Karic, and J. Jurkovic, "Uptake of heavy metals by tomato plants (Lycopersicum esculentum Mill.) and their distribution inside the plant," AgricultForest, vol. 64, no. 4, Dec. 2018.

[7] A. Ashraf, S. Bhardwaj, H. Ishtiaq, Y. K. Devi, and D. Kapoor, "Lead uptake, toxicity and mitigation strategies in plants," Plant Archives, vol. 21, no. No 1, Apr. 2021.

[8] A. L. Wani, A. Ara, and J. A. Usmani, "Lead toxicity: a review," Interdiscip. Toxicol., vol. 8, no. 2, pp. 55–64, Jun. 2015, doi: 10.1515/intox-2015-0009.

[9] N. Terry and G. S. Banuelos, "Phytoremediation of contaminated soil and water," CRC press, 2020.

[10] A. Buscaroli, "An overview of indexes to evaluate terrestrial plants for phytoremediation purposes (Review)," Ecological Indicators, vol. 82, pp. 367–380, Nov. 2017.

[11] Wu, Ming-Ling, et al. "Lead, mercury, and arsenic poisoning due to topical use of traditional Chinese medicines," The American journal of medicine 126.5 (2013): 451-454.

[12] Chen, Jian Hua, et al. "Cr (III) ionic imprinted polyvinyl alcohol/sodium alginate (PVA/SA) porous composite membranes for selective adsorption of Cr (III) ions," Chemical Engineering Journal 165.2 (2010): 465-473.

[13] J. Tang, J. Huang, T. Tun, S. Liu, J. Hu, and G. Zhou, "Cu(II) and Cd(II) capture using novel thermosensitive hydrogel microspheres: adsorption behavior study and mechanism investigation," J. Chem. Technol. Biotechnol., vol. 96, no. 8, pp. 2382–2389, Aug. 2021, doi: 10.1002/jctb.6767.

[14] X. Wang et al., "Permeable, robust and magnetic hydrogel beads: water droplet templating synthesis and utilization for heavy metal ions removal," J. Mater. Sci., vol. 53, no. 21, pp. 15009–15024, Nov. 2018, doi: 10.1007/s10853-018-2681-x.

[15] H. Ren, Z. Gao, D. Wu, J. Jiang, Y. Sun, and C. Luo, "Efficient Pb(II) removal using sodium alginate-carboxymethyl cellulose gel beads: Preparation, characterization, and adsorption mechanism," Carbohydr. Polym., vol. 137, pp. 402–409, Feb. 2016, doi: 10.1016/j.carbpol.2015.11.002.

[16] X. Song et al., "A bioinspired strategy towards super-adsorbent hydrogel spheres via self-sacrificing micro-reactors for robust wastewater remediation," J. Mater. Chem. A, vol. 7, no. 37, pp. 21386–21403, 2019, doi: 10.1039/C9TA05550A.

[17] G. Halász, B. Gyüre, I. M. Jánosi, K. G. Szabó, and T. Tél, "Vortex flow generated by a magnetic stirrer," Am. J. Phys., vol. 75, no. 12, pp. 1092–1098, Dec. 2007.

[18] C. van der Schoot and A.J.E. van Bel, "Architecture of the Internodal Xylem of Tomato (Solanum lycopersicum) with Reference to Longitudinal and Lateral Transfer," Am. J. Bot., vol. 76, no. 4, pp. 487, 1989.

[19] N. Ishtiaque Hossain and S. Tabassum, "Stem-FIT: a Microneedle-based Multi-parametric Sensor for In Situ Monitoring of Salicylic Acid and pH Levels in Live Plants," in 2022 IEEE 17th International Conference on Nano/Micro Engineered and Molecular Systems (NEMS), Apr. 2022, pp. 312–316, doi: 10.1109/NEMS54180.2022.9791212.

[20] C. Galvan, R. Montiel, K. Lorenz, J. Carter, N. I. Hossain, and S. Tabassum, "A microneedle-based Leaf Patch with IoT Integration for Real-time Monitoring of Salinity Stress in Plants," in 2022 IEEE 15th Dallas Circuit And System Conference (DCAS), Jun. 2022, pp. 1–2.

[21] N. I. Hossain and S. Tabassum, "Leaf-mounted microneedle-based multisensory platform for multiplexed monitoring of phytohormones in live plants," in Hilton Head Workshop Technical Digest, Hilton Head, SC, Jun. 2022, pp. 142–145.

CONTACT

* S. Tabassum, email: stabassum@uttyler.edu.